# Jamming and Soft-Core Rheology

**Daniel Vågberg**


**Department of Physics**
Umeå University
Umeå 2014

Department of Physics

Umeå University

SE-90187 Umeå Sweden


ISBN: 978-91-7459-784-4
Electronic version available at http://umu.diva-portal.org/
Printed by Print & Media,
Umeå University Umeå Sweden 2013

*The rule is,*
*jam tomorrow and jam yesterday,*
*but never jam today.*

— *The White Queen*

# Contents

# Sammanfattning

Jamming är en fasövergång där ett material går från en flytande vätskeliknande fas till en oordnad fast fas. Fenomenet kan observeras i en stor grupp fysikaliska system, till exempel granulära material, skum, kolloida lösningar och emulsioner. Dessa material är mycket vanliga och i princip alla industriella tillverkningsprocesser innefattar någon form av granulära råvaror, till exempel sand, träflis, frön och allehanda pulver och pellets. Att förstå hur dessa material beter sig under olika omständigheter är därför mycket viktigt av såväl vetenskapliga som ekonomiska skäl.

Dessa granulära system modelleras ofta som elastiska partiklar med repulsiva kontaktkrafter. I den här avhandligen undersöker vi flera olika modeller för att simulera granulära material. Vi undersöker bland annat effekten som olika dissipativa krafter har på systemet och studerar hur olika sätt att generera partikel-konfigurationer påverkar deras sannolikhet att "jamma" när de kyls hastigt. Vi studerar reologin hos skjuvade partikelsystem i närheten av jammingövergången. Vi använder skalningsmodeller besläktade med renormaliseringsgruppsteori för att undersöka hur olika kvantiteter skalar i närheten av den förmodade kritiska punkten J. Utifrån skalningsmodellerna bestämmer vi densiteten vid punkt J och några av de kritiska exponenter som beskriver uppförandet i närheten av denna punkt.

# Abstract

Many different physical systems, such as granular materials, colloids, foams and emulsions exhibit a jamming transition where the system changes from a liquid-like flowing state to a solid jammed state as the packing fraction increases. These systems are often modeled using soft-core particles with repulsive contact forces. In this thesis we explore several different dynamical models for these kinds of systems, and see how they affect the behavior around the jamming transition. We investigate the effect of different types of dissipative forces on the rheology, and study how different methods of preparing a particle configuration affect their probability to jam when quenched. We study the rheology of sheared systems close to the jamming transition. It has been proposed that the athermal jamming transition is controlled by a critical point, point J, with certain scaling properties. We investigate this using multivariable scaling analysis based on renormalization group theory to explore the scaling properties of the transition and determine the position of point J and some of the critical exponents.

# Publications

This thesis is based on the following publications:
(Reprints made with permission from the publishers)

I **Glassiness, Rigidity, and Jamming of Frictionless Soft Core Disks**
Vågberg, D., Olsson, P., Teitel, S.
Physical Review E. 83(3): 031307 (2011)

II **Finite-Size Scaling at the Jamming Transition: Corrections to Scaling and the Correlation-Length Critical Exponent**
Vågberg, D., Valdez-Balderas, D., Moore, M., Olsson, P., Teitel, S.
Physical Review E. 83(3): 030303 (2011)

III **Pressure Distribution and Critical Exponent in Statically Jammed and Shear-Driven Frictionless Disks**
Vågberg, D., Wu Y., Olsson, P., Teitel, S.
Manuscript submitted for publication (2013)

IV **Dissipation and Rheology of Sheared Soft-core Frictionless Disks Below Jamming**
Vågberg, D., Olsson, P., Teitel, S.
Manuscript submitted for publication (2013)

V **Universality of Jamming Criticality in Overdamped Shear-Driven Frictionless Disks**
Vågberg, D., Olsson, P., Teitel, S.
Manuscript submitted for publication (2013)

# Chapter 1

# Introduction

Rheology is the science of characterizing how a substance flows or deforms. The substance can be any soft material, from low-viscosity liquids like water to more complex substances like pastes and emulsions, or even granular materials like sand and pebbles. In this thesis we will look at the rheology of soft-core particles. Soft core indicates that the particles are soft in the sense that two particles can deform or penetrate each other if pressed together by an external force, similar to how two rubber balls deform if pressed together. We investigate several mathematical models to describe the motion of these particles under various circumstances. We are especially interested in the behavior close to what is known as the jamming transition, a liquid-solid phase transition, where the rheological properties of granular materials change dramatically.

The first part of this thesis is a brief introduction to granular materials and the jamming phase transition, after that we turn our attention to the mathematical models used to model granular materials and the assumptions they are based on. We then take a closer look at critical scaling and how it can be used in the context of the jamming phase transition and finally, we give a short summary of the included papers.

The main findings of this thesis are contained in the papers, the aim of these introductory chapters is not to repeat the content of the papers but instead to expand on some of the concepts and methods used in getting those results, which hopefully will help the reader to more easily understand the contents of the papers.

# Chapter 2

# Granular Materials and Jamming

## 2.1 What is granular matter?

Granular matter is very common in our every-day life, examples range from sand and rocks to common food items like rice, beans or more fine grained substances like table salt or ground coffee. Understanding the properties of these types of materials is important not only from an academic standpoint, but also from both a technical as well as an economical perspective. In manufacturing industry, a significant part of raw materials are at some point transported and processed either as powder or as larger grains, so any understanding that could improve the effectiveness of processing and handling of these materials would be of significant economic interest.

A granular material is a substance that consists of a large number of discrete particles or grains. The particles are usually assumed to be macroscopic in size, which means that microscopic effects such as thermal motion can be ignored. This also means that the particles motion are accurately described by classical physics and that quantum effects are negligible. Thermal motion is important for particles smaller than $\sim 1\mu m$; for larger particles the thermal motion is usually negligible and they can therefore be considered macroscopic. The shape of the particles can be arbitrary, but in this work we will only work with the simplest case which is spherical particles. One important property of granular materials is that particle interactions are dissipative, which means that energy is not conserved in the system.

In reality, if two particles collide their kinetic energy is converted to thermal energy because of the friction between the particles, but since the microscopic effects such as thermal vibrations are negligible from the perspective of a macroscopic observer, it will effectively look as if the kinetic energy in the system decreases over time.

Granular materials exhibit some very peculiar properties: the macroscopic properties of the material depend both on the detailed properties of the particles but also a lot on the surrounding environment. For example, when working with materials with small grains the macroscopic properties of the material can vary significantly with environmental parameters such as air humidity, since increased moisture changes the cohesive properties of the particles. Anyone who has ever tried to build a sand castle knows that dry sand is notoriously hard to form into structures, and that adding some water to the sand really helps the castle stick together [1]. But if one adds too much water, the properties start to deteriorate again, and if one where to construct the sand castle completely submerged under water, it would be just as hard as constructing it on land from dry sand.

The macroscopic behavior of a granular material depends a lot on how the individual grains are arranged within the system. This means that the present properties of the system depend on the history of the system. When trying to explain an effect in granular matter it is therefor important not only to ask: "What is it made of?" but also: "How did it get there?". For example, when filling a container with sand the particles may pack more or less densely depending on the details of how it is done [2]. If one, for example, wants a dense packing one can shake or vibrate the container, this will allow particles to move slightly, and because of gravity any void that appears in the lower parts of the system will quickly be filled by particles falling down into the "free" positions. This type of effect can significantly alter the macroscopic properties of the material, and this is one of the things that make granular materials interesting to work with. But it also poses a lot of challenges when trying to characterize the materials, and making reproducible measurements. In paper I we look at one

aspect of this where we compare particle configurations generated in different ways. Another related phenomenon that appears when a container of granular materials is vibrated is what is known as the Brazilian nut effect that we will discuss in section 4.3.1.

## 2.2 Jamming

One of the phenomena that can be observed in granular matter is jamming. A system of granular material is said to be jammed if it exhibits a non-zero yield stress. A non-zero yield stress means that the system of particles can withstand the action of a force without collapsing, this is the signature of a solid substance. If the system is not jammed, the particles will rearrange when subjected to the force, and the material will behave more like a fluid. In figure 2.1 we see a typical situation where jamming is likely to occur: particles are flowing out from a container through a funnel with a narrow opening. This is the typical textbook example of jamming. The probability of forming an arch spanning the opening and blocking the flow is strongly dependent on the size of the opening [3]. The decreasing diameter of the funnel near to the opening forces the particles to get closer to each other, further increasing the likelihood of forming jammed structures that block the flow. In this setting jamming is usually considered a problem. However, there are many emerging applications where jamming is used in a controlled way to manipulate flows and rigidity of objects, for example as actuators in robots [4].

It turns out that the probability of jamming is closely connected to the packing fraction $\phi$ of the material, the packing fraction is a measure of how densely stacked the particles are. The packing fraction for a system of $N$ particles is given by

$$\phi = \frac{\sum_{i=1}^{N} V_i}{V} \tag{2.1}$$

where $V_i$ is the volume of particle $i$ and $V$ is the total volume of the container. This applies for a three-dimensional system. For a

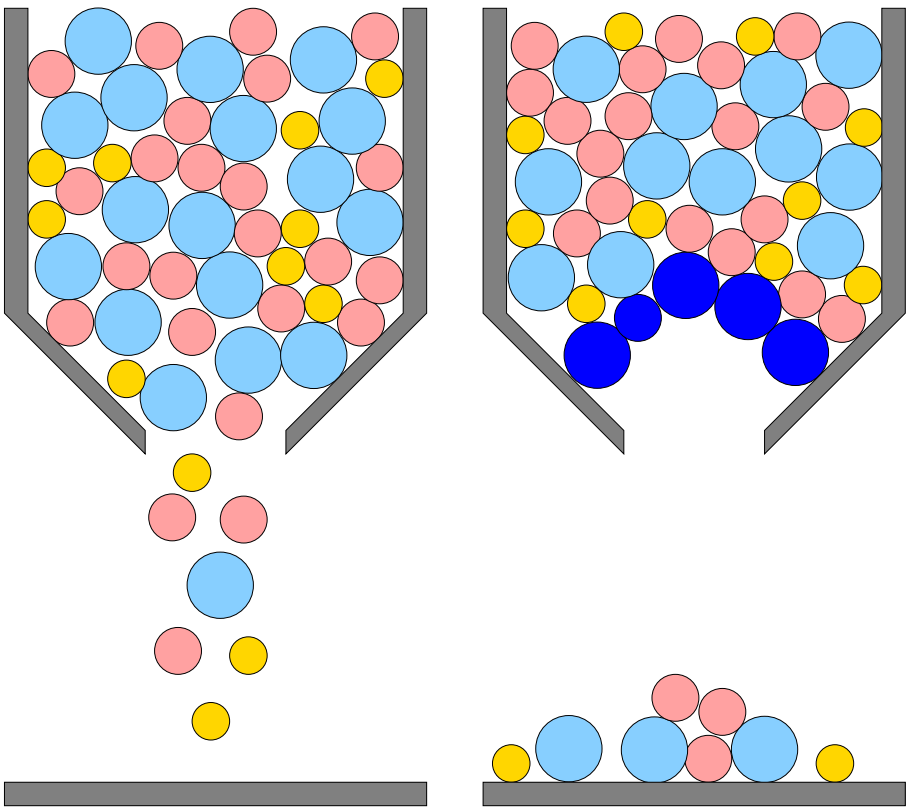

(a) Flowing (b) Jammed

Figure 2.1: Granular flow trough a constriction in a pipe. (a) Initially the material flows through the opening but after some time (b) the the flow stops and the system jams as a load-bearing arch forms across the opening. The particles forming the arch have been highlighted in panel (b).

two-dimensional system one would of course use the area instead of the volume. It turns out that a system of particles at low $\phi$ is fluid, while at high $\phi$ the system jams and becomes rigid. The physics in the transition region where the system transitions between these two states is highly non-trivial, and understanding this transition is a very active research field.

## 2.3 Jamming as a Phase Transition

The jamming phenomenon and other similar effects can be observed in a wide variety of systems, not only in granular materials. Other disordered liquid-to-solid transitions are for example the glass transition were we have a temperature-dependent transition, or the flow of more cohesive systems like foams and emulsions, which have finite yield stress and require some minimum applied force to start flowing. In 1998, Liu and Nagel [5] proposed a way to unify all of these systems by combining them as different planes in a common phase diagram, see figure 2.2. The phase diagram has three axes, temperature $T$, inverse packing fraction $\phi^{-1}$, and stress $\sigma$. Together these three axes divide the phase space into two regions, one jammed region close to the origin, surrounded by an unjammed outer region. In the $T - \phi^{-1}$ plane we have the glass transition, and in the $\phi^{-1} - \sigma$ plane we have the athermal jamming transition for driven granular materials. Point J in figure 2.2 is a critical point located at the packing fraction $\phi_J$. Originally it was thought that point J would govern the behavior of both the athermal jamming transition and the equilibrium glass transition, however it has later been shown that the glass transition is a separate transition occurring at $\phi_G < \phi_J$ and controlled by a separate critical point [6] [7].

Most of the work in this thesis have been done in the vicinity of point J. Since the point is located on the $\phi^{-1}$ axis with $T = 0$ and $\sigma = 0$, it is difficult to access the point directly with simulations. Since the dynamics of granular matter is dissipative, in order to get a

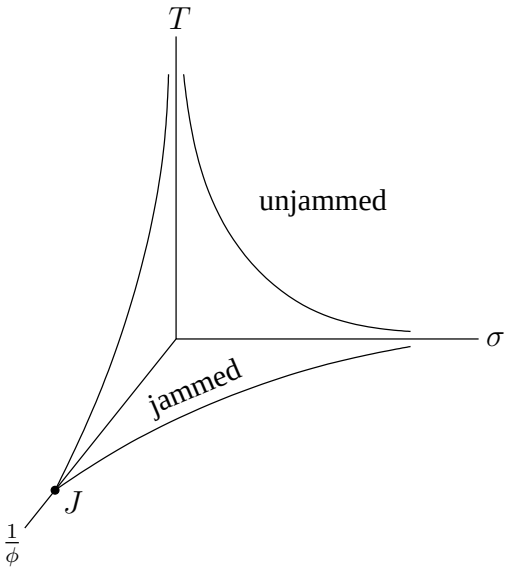


Figure 2.2: The jamming phase diagram.

dynamic system to measure we have to drive/excite the system. In our case we have mainly used shearing to drive the system. We drive the system by shearing at a constant shear strain rate $\dot{\gamma}$, see section 4.2.3 for more details on how this can be implemented. The shear causes the particles to move relative to each other which leads to non-zero stresses $\sigma$ in the system.

The exact value of $\phi_J$ is dependent on the details of the studied system. Factors like particle shape, the size distribution of the particles, amount of friction between the particles and the dimensionality of the system all affect the value of $\phi_J$. For spherical particles on finds that $\phi_J \approx 0.84$ in two dimensions and $\phi_J \approx 0.64$ in three dimensions. We can compare this to the corresponding values for ordered close-packing of spheres, which for two dimensions is the triangular lattice with $\phi_{\text{cp}} = \pi/(2\sqrt{3}) \approx 0.907$, and in three dimensions $\phi_{\text{cp}} = \pi/\sqrt{18} \approx 0.740$ using either the fcc- or hcp-lattice. Since a jammed system by definition is disordered, $\phi_J$ will always be lower

than the corresponding $\phi_{\text{cp}}$.

## 2.4 Critical Scaling

Physicists have over time built up a large theoretical framework within the fields of statistical physics and thermodynamics for working with phase transitions, however most of that work has been on systems in equilibrium. Since the athermal jamming phase transition requires driving in order to explore phase space, it is per definition a non-equilibrium phenomenon. It is currently unclear how well this type of non-equilibrium transition will fit into the existing theoretical framework for equilibrium transitions. But there is an increasing amount of work [8–10] suggesting that the transition shares many properties of a continuous phase transition.

One of the hallmarks of equilibrium critical points is the notion of *universality*; the critical behavior, specifically the exponents describing the divergence or vanishing of observables, depend only on the symmetry and dimensionality of the system, and not on details of the specific interactions.

If point J is a critical point, we would expect the system to exhibit critical scaling which means that many quantities start to obey power laws as we get closer to point J. What this means is that the behavior of an observable $\mathcal{O}$ approaching the critical point J from below could be written in the form

$$\mathcal{O}(\phi) = (\phi_J - \phi)^{q_\mathcal{O}}, \tag{2.2}$$

where $\phi_J$ is the critical packing fraction, i.e. the location of point J, above which the system is jammed. Here $\phi_J - \phi$ is the distance from the critical point and $q_\mathcal{O}$ is the critical exponent associated with the observable $\mathcal{O}$. Each critical point is characterized by a set of critical exponents. These critical exponents serve as a finger print that can be used to classify the phase transition into what is known as universality classes. All transitions with the same critical exponents are said to belong to the same universality class.

The region in which the critical behavior can be observed is usually rather small so in order to measure the critical exponents with some accuracy, one has to get good data fairly close to the critical point, and this can be a challenge both in real-world experiments and in computer simulations.

From traditional thermodynamic phase transitions one would expect that the values of the critical exponents are fairly robust and that small changes in the microscopic interactions should not change the universality class of the transition. However, for the jamming transition thing seem to be a bit more complicated. In 2003 O'Hern et al. [11] showed that some exponents depend on the form of the interparticle potential. The exponents are also sensitive to the way the system is driven, as we show in paper II and III, where the critical exponents differ between sheared and compressed systems.

The scaling shown in equation (2.2), is a limiting case where we assumed that only the $\phi$ parameter is important, in reality the dynamics may depend on more variables, i.e. $T$ and/or $\dot{\gamma}$ depending on how we drive the system, and $L$, which is the size of the simulated system. In chapter 5 we will look closer at the full scaling relations that are used for analyzing the data in the papers.

## 2.5 The coordination number $z$

The coordination number $z$, also known as the contact number, is the average number of contacts per particle. Two particles are said to be in contact if they are close enough that they touch one another. In the previous sections we have introduced jamming in terms of the packing fraction $\phi$, it is also possible to look at jamming from the perspective of the contact number. When we increase $\phi$ the particles get closer together and eventually jam as $\phi \geq \phi_J$. As the particles get closer more contacts are formed which means that $z$ increases and that the system jams as $z \geq z_J$.

It turns out that under some circumstances it is possible to calculate

$z_J$ exactly. The argument goes as follows. In order for the system to jam and form a stable (rigid) mechanical structure the particles have to be sufficiently constrained. If we know the number of particles and the number of degrees of freedom for each particle we can calculate the total number of variables needed to specify the state of the system. In order to get a stable mechanical structure we need at least as many equations as unknown variables in the system. When the number of equations exactly matches the number of unknown variables, the system is said to be isostatic. A configuration of frictionless particles is believed to be isostatic exactly at the jamming transition [12].

For the following argument we are going to need a stricter definition of $z$. We define $Z$ to be the average number of contacts per particle but this time we first remove so called rattlers (free particles that are not part of the jammed force-network) from the system before calculating the average. For each particle we should have force balance and torque balance, the number of equations needed to achieve this depends on the number of degrees of freedom for each particle. For spherical particles in $D$ dimensions dimension we get $Z_{\text{iso}} = 2D$ in the absence of friction, and $Z_{\text{iso}} = D + 1$ if the friction coefficient $\mu \to \infty$. which means spherical particles with finite friction will jam somewhere in the interval $D + 1 \leq Z_J \leq 2D$, the exact point depend on the details of the specific particle configuration. For non-spherical particles $Z_{\text{iso}}$ increases as the rotational symmetry is broken. From the previous argument one would expect $Z_{\text{iso}}$ to change discontinuously as the symmetry is broken, however in reality the number of contacts increases continuously as the shape is varied [13, 14]. This effect can be explained with some more careful analysis [15].

# Chapter 3

# Rheology

Rheology is the science that describes how substances flow and deform. The study of rheology is normally aimed at describing the flow properties of liquids and other soft materials, such as granular materials. However, even materials we normally consider solid can be made to flow, given extreme enough circumstances. Rheology is a large subject and this chapter will only be a quick introduction to the most common rheological behaviors which one are likely to encounter while working with granular materials. We will focus on the rheology of sheared systems.

## 3.1 Elastic Solids

The simplest model of a solid is a linear elastic solid in which deformations follow Hooke's law. Here the deformation of the substance will be proportional to the applied stress $\sigma$. Once the stress is removed the system will return to its original shape. In reality this behavior is only observed for small stresses/deformations; a real material will start to deform permanently once the stress reaches a material-specific threshold value known as the yield stress $\sigma_Y$. If $\sigma > \sigma_Y$ the material will plastically deform and will not return to the original configuration when the stress is removed. In the elastic region the relation between the shear strain, $\gamma$, and the stress is given by

$$\sigma = G\gamma \tag{3.1}$$

where $G$ is the shear modulus. We expect to see this behavior in jammed systems of granular material. Jammed materials are in gen-

eral fragile and particle rearrangement will occur if $\sigma > \sigma_Y$.

## 3.2 Newtonian Fluids

Normal liquids such as water are known as Newtonian fluids which means that their flow can be described by a single parameter, the viscosity $\eta$. The shear viscosity of a Newtonian fluid is given by

$$\eta = \frac{\sigma}{\dot{\gamma}}. \tag{3.2}$$

Here we see that $\sigma \sim \dot{\gamma}$ in a Newtonian fluid. Below the jamming transition we expect the system to exhibit a linear (Newtonian) rheology if the particle dynamics is overdamped. See paper IV for more details on when a system can be considered to be overdamped.

## 3.3 Non-Newtonian Fluids

Non-Newtonian fluids, i.e. fluids that do not flow according to equation (3.2), includes a large group of materials which shows a wide variety of phenomena. One example is Bingham plastics, a type of viscoplastic materials [16]. These materials have a low but finite yield stress, at higher stresses the material flows at a rate which is proportional to the part of the stress that exceeds the yield stress. One such material is mayonnaise, which is a type of emulsion.

Other interesting effects can be seen in materials where the viscosity is not linearly dependent on the shear rate. A material where the apparent viscosity decreases at high shear rates is said to exhibit shear thinning, and a material where the apparent viscosity increases at high shear rates is said to exhibit shear thickening.

A striking example of shear thickening is found when corn starch is suspended in water. Any reader that has not had the opportunity to study this kind of systems are encouraged to do some kitchen science. At low shear rate this suspension is flowing like a liquid, but for

higher shear rates the viscosity rapidly increases to the point where the material turns almost solid.

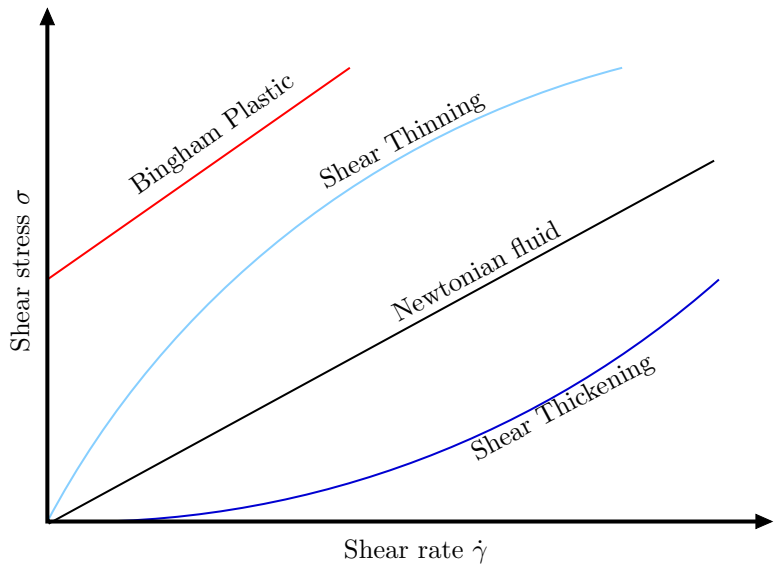


Figure 3.1: Schematic diagram of the relation between shear stress and shear strain rate for different types of fluids.

Figure 3.1 illustrates how the shear stress depends on the shear rate in the above-mentioned systems. This is in no way a complete list of non-Newtonian effects, however, the flow types mentioned in figure 3.1 includes the most common effects that one is likely to observe when studying granular materials.

The rheology of dry granular materials often exhibits shear thickening below jamming. If we ignore the effects close to the critical point, one finds that the shear stress $\sigma \sim \dot{\gamma}^2$, this indicates that the dynamics is not overdamped and that inertial effects are important for the dynamics. The effect was first observed by Bagnold in 1954 [17] and his name is often used to refer to this type of dynamics.

# Chapter 4

# Numerical Models

In this chapter we will look at some of the different numerical approaches used to simulate granular materials. This is a big subject and we will therefore mainly focus on the methods used in the papers. Other methods will be mentioned briefly where appropriate to highlight pros and cons of the methods used in the papers.

## 4.1 Common Notation

We will consider two dimensional, $D = 2$, systems of soft-core circular particles usually in a bidisperse mixture in order to avoid crystallization. There are $N$ particles in the system. Each particle $i$ is described by a position $\mathbf{r}_i$, a velocity $\mathbf{v}_i$ and a radius $R_i$. The distance between two particles $i$ and $j$ is $r_{ij} = |\mathbf{r}_{ij}|$ where $\mathbf{r}_{ij} = \mathbf{r}_i - \mathbf{r}_j$ and the sum of their radii $d_{ij} = R_i + R_j$. If $r_{ij} < d_{ij}$ the particles are touching and the size of the overlap is given by $d_{ij} - r_{ij}$. The direction of the unit vector $\hat{\mathbf{r}}_{ij} = \frac{\mathbf{r}_{ij}}{r_{ij}}$ is consistent with a repulsive radial contact force.

## 4.2 Shearing and Boundary Conditions

In many models of granular materials there is no temperature, $T = 0$, and the dynamics is often dissipative, which means that any kinetic energy in the system will dissipate over time, leading to a stationary state. This means that in order to get a dynamic behavior to study, we need to perturb or drive the system in some way. One way to drive the system is to shear it. Shear could be seen as a deformation of

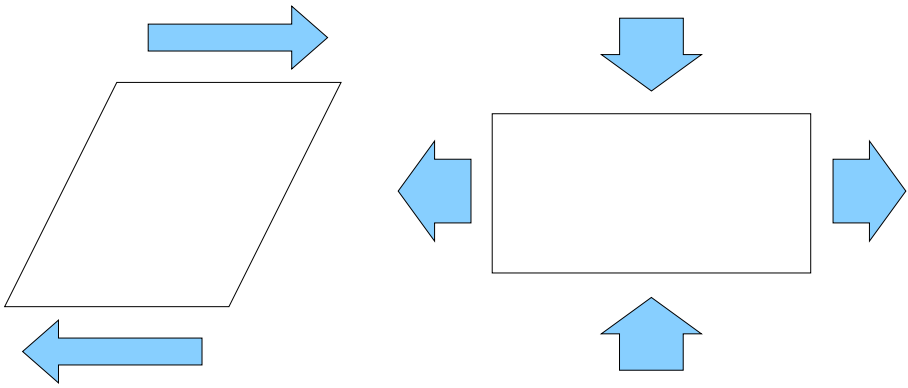

(a) Simple shear

(b) Pure shear

Figure 4.1: Schematic view of shear deformations.

the system where we change the shape of the simulated system while keeping the area constant. There are two main types of shearing: simple shear and pure shear. Figure 4.1 shows schematic diagrams of the two different types of shear deformations. We use simple shear to drive our system.

In the simulations we use two types of boundary conditions. When there is no shear applied to the system we use normal periodic boundary conditions, but in order to shear the system we need to modify the boundaries. There are several ways of applying simple shear to a system. We use what is known as Lees-Edwards boundary conditions [18]. In the following section we will take a closer look at the boundary conditions we use and also look at some alternative ways of shearing the system.

### 4.2.1 Periodic Boundary Conditions

Periodic boundaries is a standard approach which the reader probably already is familiar with, it is included here mainly as a reference when comparing with the more specialized boundaries used when shearing the system. Figure 4.2 shows the main idea with periodic boundary

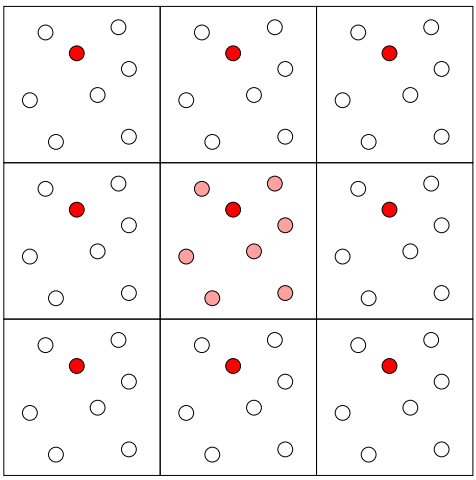

Figure 4.2: Periodic boundary conditions.

conditions. The particles we actually simulate are represented by the shaded circles in the middle box. This is our simulation cell. We assume that the central cell is surrounded by identical cells, repeated periodically in all directions. To illustrate this, one particle in the figure has been highlighted, so one easily sees where the periodic images of this specific particle are located. What this means in practice, is that if a particle leaves the cell by passing the cell boundary at one side of the cell, it will instantly reappear on the opposite side of the cell.

Periodic boundaries are often used in order to limit the boundary effects. If we instead of periodic boundaries had a box with solid walls, a particle close to the wall would be restricted in the way it could move, and would behave slightly differently than a particle far away from the wall. Using periodic boundary conditions this boundary effect disappears and all particles experience the same environment independent on where in the system they are located. This makes the system in many respects appear bigger than it actually is. However, the system is still of finite size and depending on what type of system

one studies, there could still be finite size effects affecting the dynamics of the system.

### 4.2.2 Shearing by sliding walls

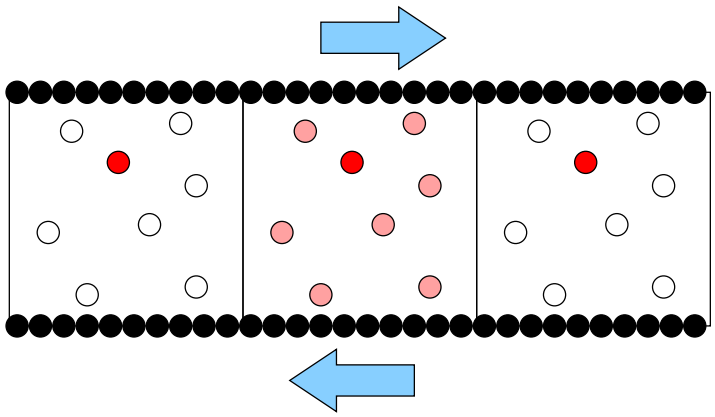

Figure 4.3: Shearing with moving walls.

Moving walls is a straight-forward method of adding shear to a system. The main idea is to use a system which is periodic along one axis, and closed off by walls in the other direction, see figure 4.3. The shear is then added by actively sliding the two walls relative to each other. For this to work there must be friction between the wall surface and the particles in the system. One common way of achieving this is to construct the walls as a row of fixed particles with similar size and properties as the free particles in the system. This gives a wall with a rough surface which will work even in models without any explicit friction term.

Since the shear force from the wall only directly affects the particles located right next to the walls, it takes some (finite) amount of time for the shearing motion to reach the central part of the system. This means that we can observe what is known as shear banding where different parts of the system experience different shear rates. This is

normally a transient effect; if the walls move at constant velocity the central part of the system will eventually catch up and experience the same shear as the rest of the system.

### 4.2.3 Lees-Edwards Boundary Conditions

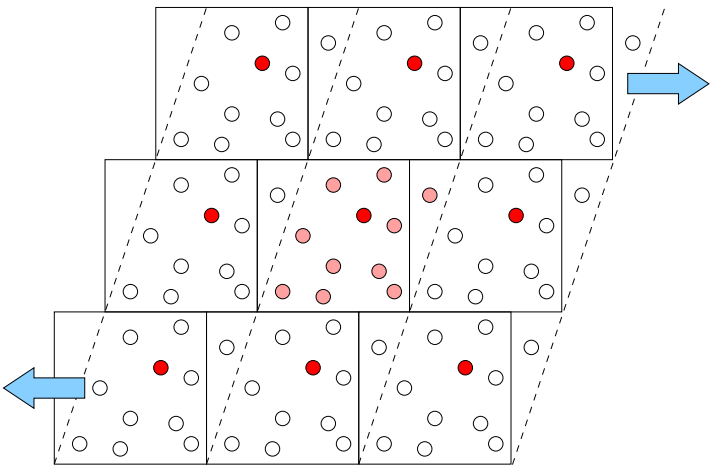

Figure 4.4: Lees-Edwards boundary conditions.

The Lees-Edwards boundaries is a clever way to shear the system and still maintain most of the benefits of periodic boundaries in both directions. The idea is to have ordinary periodic boundaries in one direction, while in the other direction periodic images of each particle are displaced. The concept is illustrated in figure 4.4, where we see that the three rows are displaced relative to each other. The system experiences shear whenever the displacement between the different rows changes. In order to avoid a sharp velocity gradient at the system boundary, the particle positions are interpolated across the system. This is indicated by the dashed lines in 4.4, and is accomplished through a clever coordinate transformation, described below. The benefit of this method is there are no boundary effects and all particles in the simulation experience the same environment.

One difference between this method and the sliding wall approach is that the shear is done by directly imposing a displacement by a coordinate transformation rather than by applying a force that then causes the particles to move. Another effect of this is that a change in shear rate is visible to the whole system immediately. This effectively prevents the formation of shear banding.

### 4.2.4 The sheared coordinate system

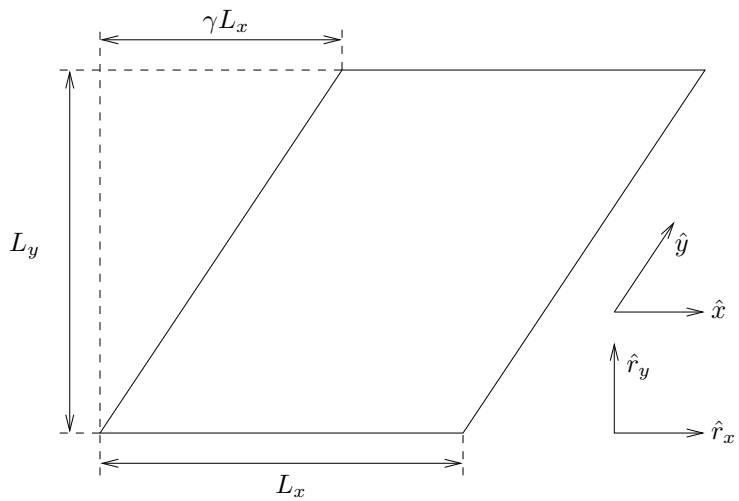


Figure 4.5: Sheared simulation cell using Lees-Edwards boundary conditions. The cell has size $L_x \times L_y$, the cell have been sheared so that the upper and lower part of the cell have been displaced a total of $L_x\gamma$

When implementing Lees-Edwards boundary conditions one introduces a special sheared coordinate system. In the simulation we use two different coordinate systems. We let $r_x$ and $r_y$ refer to the lab frame, the real physical coordinates of the particles, while $x$ and $y$ are the sheared coordinates that are used to facilitate the shearing of the

system. The two coordinate systems are related as follows:

$$\begin{cases} r_x = x + \gamma y, \\ r_y = y. \end{cases} \tag{4.1}$$

The relation between the two systems is also shown in figure 4.5. The coordinate axis for the $r_x$ and $r_y$ coordinates are always fixed, while the direction of the $y$-axis shifts as the shear strain $\gamma$ changes. The particle positions are stored in the $x$-$y$-coordinates so when $\gamma$ changes the physical positions of all particles are automatically modified. An important quantity here is the shear strain rate,

$$\dot{\gamma} = \frac{d\gamma}{dt}, \tag{4.2}$$

which controls how fast the system is sheared. Using this setup it is possible to shear the system to arbitrary large strains $\gamma$. However, numerically the value of $\gamma$ is usually kept in the interval $0 < \gamma < 1$. When $\gamma = 1$ we can utilize the symmetry in the system and transpose the triangular right half of the system to the left side of the system, forming a physically equivalent configuration with $\gamma = 0$ from which we can continue shearing. The same type of technique can also be used to keep $\gamma$ in other intervals e.g. $-0.5 < \gamma < 0.5$, which is what we use in our simulations.

Using the sheared coordinates we can define the lab-frame velocity as

$$\begin{cases} v_x = \dot{r}_x = \dot{x} + \dot{\gamma} y + \gamma \dot{y}, \\ v_y = \dot{r}_y = \dot{y}. \end{cases} \tag{4.3}$$

One is often interested in how much the velocity is deviating from the affine shear velocity given by $\dot{\gamma} y$. It is then convenient to work with the modified velocities $\mathbf{u}$ which are defined as

$$\begin{cases} u_x = v_x - \dot{\gamma} y, \\ u_y = v_y. \end{cases} \tag{4.4}$$

A particle with $u_x = 0$ follows the velocity profile of the shear flow exactly. Note that the modified velocities are not simply $(\dot{x}, \dot{y})$, instead we get:

$$\begin{cases} \dot{x} = \dot{r}_x - \dot{\gamma} r_y - \gamma \dot{r}_y = v_x - \dot{\gamma} y - \gamma v_y = u_x - \gamma u_y, \\ \dot{y} = \dot{r}_y = v_y = u_y. \end{cases} \tag{4.5}$$

## 4.3 Particle Properties

### 4.3.1 Distribution of Particle Sizes

The distribution of particle sizes affects the properties of the resulting granular material. One usually distinguishes between three types of distributions. A granular material can be either: monodiperse, meaning that all particles have the same size, bidisperse, meaning that the material consists of particles with two different sizes, or polydisperse, meaning that the system consists of more than two different particle sizes.

One effect that can be observed if particles with different sizes are mixed together is phase separation, where the dynamics under some circumstances can make particles of different sizes separate and end up in different parts of the system. One example of that would be gravity acting on particles in a container. If the particles are disturbed by some external force vibrating the container, small particles will start to migrate to the bottom while large particles rise to the top [19]. This is known as the Brazilian nut effect, since the size separation effect can often been seen when handling bags containing nuts of different sizes.

Another size-dependent effect is crystallization. Even though the materials we consider do not have any attractive forces between the particles, the dynamics may still favor a crystal-like ordered state. If we once again consider a container with particles and vibrate the container under the influence of gravity, the packing will compactify as the vibrations causes particles to rearrange. If all particles have the same size they will begin to arrange themselves in ordered layers, and

the packing will approach a close-packed crystalline state. One thing to mention here is that the size of the container is also of some importance, the system crystallizes more easily if the length of the container is an integer multiple of the particle size. For bi- and polydisperse system, crystallization is in general more difficult, but the probability to form crystals depends on the specific combination of particles sizes.

In our simulations there is no gravity, but we instead shear the system, a driving mechanism that under some circumstances can also lead to the formation of ordered layers. These effects can be good or bad depending on what property of the system one would like to study. In our case, since we want to study the behavior of disordered systems, both crystallization and phase-separation are unwanted effects which we strive to avoid. This is achieved by using a bidisperse system, where the ratio between the diameter of the large and small particles have been specifically selected to suppress crystallization [20, 21]. We use a mixture of equal number of large and small particles with a diameter ratio of 1.4.

The difference between using mono- and bidisperse particles is shown in figure 4.6 and 4.7. Each figure shows two particle configurations, before and after shearing. Initially, both configurations are disordered. The two systems are then sheared at a constant shear rate for the same amount of time. From the resulting configurations one sees a clear difference between the monodisperse configuration where the particles align and the bidisperse system which remains disordered. Crystallization of monodisperse systems happens very quickly when shearing a two dimensional system. For simulations in three dimensions, crystallization is less likely, but the effect can still be observed, especially in small systems [22].

### 4.3.2 Soft Core vs Hard Core - The Inter-particle Potential

When selecting a model for simulating granular materials one important aspect is to choose what type of particles to use. There are basically two classes of particles: hard and soft.

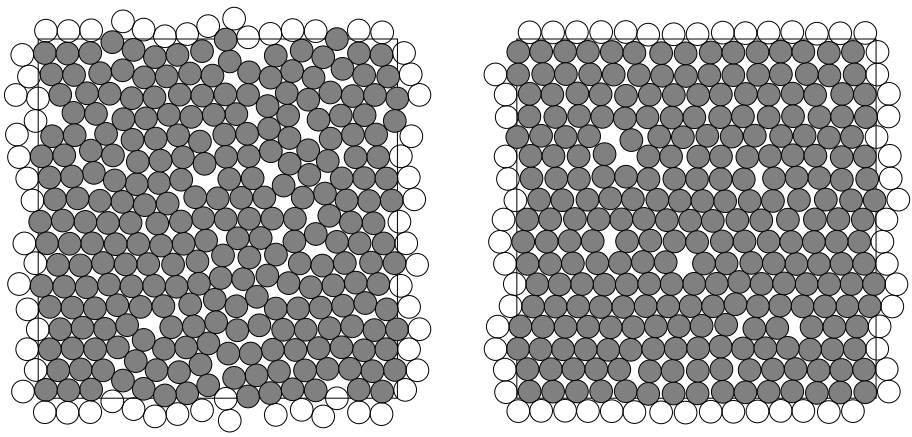

(a) Monodisperse $t = 0$ (b) Monodisperse $t = 10^5$

Figure 4.6: A monodisperse configuration with $N = 256$ particles, at $\phi = 0.8$, before and after shearing for $t = 10^5$ time units at $\dot{\gamma} = 10^{-3}$. The shearing rapidly aligns the particles into crystal planes sliding against each other. Once the particles have aligned into planes the configuration will remain in a low energy ordered state, it is highly unlikely that the system would revert back to a more disordered high energy state.

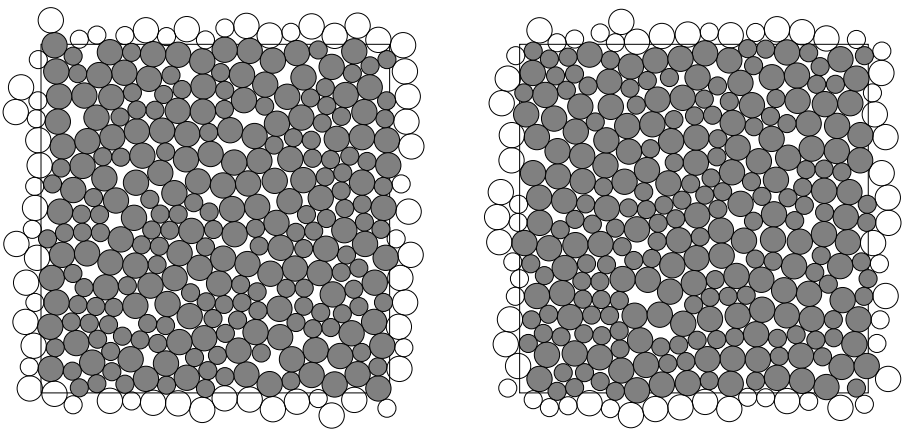

(a) Bidisperse $t = 0$ (b) Bidisperse $t = 10^5$

Figure 4.7: A bidisperse configuration with $N = 256$ particles at $\phi = 0.8$, before and after shearing for $t = 10^5$ time units at $\dot{\gamma} = 10^{-3}$. The diameter ratio between the large and the small particle is 1.4, configuration contains equal numbers of large and small particles. Here the different radii makes it difficult to form a regular lattice and the system remains disordered even after long simulations of continuous shearing.

A hard particle consists of an infinitely stiff material. This means that two hard particles can never overlap or deform, and that a collision between two such particles is instantaneous. These are of course mathematical idealizations and there are no perfectly hard particles in the real world, but particles made out of hard relatively incompressible materials such as steel behave almost like hard particles under normal conditions, but its all a matter of which parameters one uses since even a steel ball will deform given enough pressure. More formally, the hard-core potential between two particles is defined as

$$V(r_{ij}) = \begin{cases} \infty, & \text{for } r_{ij} < d_{ij}, \\ 0, & \text{for } r_{ij} \geq d_{ij}. \end{cases} \tag{4.6}$$

Soft particles, on the other hand, are allowed to deform or overlap, i.e. they behave more like soft rubber balls. In simulations one usually keeps the particle shape fixed (i.e. no deformations), but instead allows two colliding particles to penetrate each other, the force between the two particles is then based on the size of the particle overlap. The exact expression for this force and how it depends on the size of the particle overlap will give a wide variety of different types of soft particles with different properties. In our simulation we use this interaction potential

$$V(r_{ij}) = \begin{cases} \frac{k_e}{\alpha}\left(1 - r_{ij}/d_{ij}\right)^{\alpha}, & \text{for } r_{ij} < d_{ij}, \\ 0, & \text{for } r_{ij} \geq d_{ij}, \end{cases} \tag{4.7}$$

where $k_e$ is a coupling constant which can be used to adjust the strength of the potential, and the exponent $\alpha$ controls the stiffness of the potential. For most simulations we use $\alpha = 2$ which give a one-sided harmonic potential. In some cases we also use $\alpha = 2.5$, the Hertzian potential. The reason for using the Hertzian potential is that it more closely matches the potential observed in experiments on real granular materials [23]. However, in many cases that degree of realism is not needed, and since the harmonic potential is faster to compute and gives simpler expressions, it is usually preferred. When investigating the universality of the jamming transition it is also useful to

test different potentials as the critical behavior is dependent on the parameter $\alpha$ [11, 24] something we also observe in paper III.

A significant difference compared to hard particles is that for soft particles the collision takes a finite amount of time. This has far-reaching consequences for how the numerical simulation of these systems are done. For hard particles at finite temperature, one typically uses event-driven simulations where each particle collision is handled exactly, there is no fixed time step since the exact time of the next collision can be calculated based on the current particle positions and velocities. One can then advance the system to that time, solve the collision, and then calculate when the next collision will occur and so on [25].

There are also methods for simulating hard-core particles at zero temperature. In that case contacts last a finite amount of time and the normal hard core dynamics can not be used. One such method is described by Lerner et al. in Ref. [26].

For soft particles collisions take a finite amount of time, which means that several contacts are present at the same time. The normal way to advance a system of soft particles in time is therefore to numerically integrate the equations of motion using some standard finite differential method to step forward in time with a small time step $\Delta t$.

Since soft-core particles are allowed to overlap, it is possible to simulate systems at packing fractions above the jamming transition, $\phi_J$. This means that it is possible to study the transition while approaching $\phi_J$ both from above and below. Simulations using hard-core particles are limited to packing fractions below jamming.

## 4.4 Soft-Core Particle Dynamics

Here we will take a closer look at the models used in the articles to represent our granular material. In all models the particles have been modeled using a repulsive potential with frictionless contacts. The dissipation has been modeled using different types of viscous forces.

We have studied both massive particles (paper IV and V) and overdamped models where the particles do not have any mass (paper I, II and III). In the studied models the particles have no rotational degree of freedom. With the exception of the Monte Carlo simulations in paper I, all simulations have been at temperature $T = 0$.

## 4.5 The Durian Bubble Model

In 1995 Durian presented a model for simulating bubbles using overdamped soft-core particles [27] sheared using Lees-Edwards boundary conditions. In this model there are two forces acting on a given particle $i$, first an elastic force $\mathbf{f}_i^{\text{el}}$ given by

$$\mathbf{f}_i^{\text{el}} = -\sum_{j \neq i}^{N} \nabla V(r_{ij}), \tag{4.8}$$

created by some inter-particle potential (in our case Eq. (4.7)), and $\mathbf{f}_i^{\text{dis}}$ which is the dissipative force, which we will define shortly. From Newton's second law we normally get the equations of motions as

$$m_i \ddot{\mathbf{r}}_i = \mathbf{f}_i^{\text{el}} + \mathbf{f}_i^{\text{dis}}, \tag{4.9}$$

where $m_i$ is the mass of particle $i$. However since this model has overdamped dynamics, which corresponds to the limit $m \to 0$, we instead base our equation of motions on the following force balance

$$\mathbf{f}_i^{\text{el}} + \mathbf{f}_i^{\text{dis}} = 0. \tag{4.10}$$

Durian describes two versions of this model using different expressions for $\mathbf{f}_i^{\text{dis}}$. In the following sections we will look at both these models, which we refer to as $\text{CD}_0$ and $\text{RD}_0$, where CD stands for Contact Dissipation, and RD for Reservoir Dissipation. The "0" indicates that $m = 0$, which means that the models are overdamped.

### 4.5.1 The $CD_0$ model

The dissipative force is modeled as a viscous drag force. Durian suggested two different expressions for $\mathbf{f}_i^{\text{dis}}$, first the more general

$$\mathbf{f}_i^{\text{dis}} = -k_d \sum_{r_{ij}<d_{ij}} (\mathbf{v}_i - \mathbf{v}_j), \tag{4.11}$$

where the sum only runs over particles $j$ in contact with $i$. Here $k_d$ is a coupling constant that can be used to adjust the strength of the dissipation. If we plug in this expression for $\mathbf{f}_i^{\text{dis}}$ in (4.10) we get the following implicit formula for the velocity

$$\mathbf{v}_i = \frac{1}{z_i} \sum_{r_{ij}<d_{ij}} \mathbf{v}_j + \frac{1}{z_i k_d} \mathbf{f}_i^{\text{el}}, \tag{4.12}$$

where $z_i$ is the number of particles in contact with particle $i$. In order to solve for the velocity we have to rewrite this in matrix form. We define vectors containing the values for all $N$ particles: $\mathbf{v_x} = (v_{x0}, v_{x1}, ..., v_{xN-1})$ and $\mathbf{f_x} = (f_{x0}^{\text{el}}, f_{x1}^{\text{el}}, ..., f_{xN-1}^{\text{el}})$, and similarly for the other component $\mathbf{v_y}$ and $\mathbf{f_y}$. We can then rewrite (4.12) as

$$\begin{cases} \mathbb{A}\mathbf{v_x} = \frac{1}{k_d}\mathbf{f_x}, \\ \mathbb{A}\mathbf{v_y} = \frac{1}{k_d}\mathbf{f_y}, \end{cases} \tag{4.13}$$

where the matrix $\mathbb{A}$ is defined as

$$\mathbb{A}_{ij} = \begin{cases} z_i, & \text{for } i = j, \\ -1, & \text{for } i \neq j \text{ and } r_{ij} \leq d_{ij}, \\ 0, & \text{for } r_{ij} > d_{ij}. \end{cases} \tag{4.14}$$

Since the matrix only contains equations describing the relative velocity between the particles, the matrix is singular and there is no unique solution. The physical meaning is that there is nothing in equation 4.12 that prevents all particles from simultaneously translate at arbitrary speeds in a common direction. In order to get a unique solution

we need to add further constraints. This can be done by a slight modification to the model where we add a small friction term $\delta \ll 1$ between the particles and the background substrate. We can then redefine the matrix $\mathbb{A}$ as

$$\mathbb{A}_{ij} = \begin{cases} z_i + \delta, & \text{for } i = j, \\ -1, & \text{for } i \neq j \text{ and } r_{ij} \leq d_{ij}, \\ 0, & \text{for } r_{ij} > d_{ij}. \end{cases} \tag{4.15}$$

Using this approach we are guaranteed that $\mathbb{A}$ will always be invertible. The above equations can be used directly if the system is not periodic in the $y$-direction, but they need some adaptations in order to fulfill the Lees-Edwards boundary conditions. We can get the correct form for Lees-Edwards boundary conditions by rewriting Eq. (4.11) using the modified velocities,

$$\begin{aligned} \mathbf{f}_i^{\text{dis}} &= -k_d \sum_{r_{ij}<d_{ij}} (\mathbf{v}_i - \mathbf{v}_j) - k_0 \mathbf{v}_i \\ &= -k_d \sum_{r_{ij}<d_{ij}} \left(\mathbf{u}_i - \mathbf{u}_j + \dot{\gamma}[y_i - y_j]_{L_y}\hat{\mathbf{x}}\right) - k_0(\mathbf{u}_i + \dot{\gamma} y_i \hat{\mathbf{x}}) \\ &= -k_d \sum_{r_{ij}<d_{ij}} \mathbb{A}_{ij}\mathbf{u}_j - k_d\dot{\gamma} \sum_{r_{ij}<d_{ij}} [y_i - y_j]_{L_y}\hat{\mathbf{x}} - k_0 \dot{\gamma} y_i \hat{\mathbf{x}}. \end{aligned} \tag{4.16}$$

Here the friction term has been included and we can identify $\delta = k_0/k_d$. The notation $[y_i - y_j]_{L_y}$ stands for the shortest distance between $i$ and $j$ in the $y$ direction, considering the periodic boundary conditions. We then insert Eq. (4.16) into Eq. (4.10) and rewrite the expression in vector form as

$$\begin{cases} \mathbb{A}\mathbf{u}_\mathbf{x} = \frac{1}{k_d}\tilde{\mathbf{f}}_\mathbf{x}, \\ \mathbb{A}\mathbf{u}_\mathbf{y} = \frac{1}{k_d}\mathbf{f}_\mathbf{y}, \end{cases} \tag{4.17}$$

where the components of $\tilde{\mathbf{f}}_\mathbf{x}$ are given by

$$\tilde{f}_i x = f_{ix}^{\text{el}} - k_d\dot{\gamma} \sum_{r_{ij}<d_{ij}} [y_i - y_j]_{L_y} - k_0 \dot{\gamma} y_i. \tag{4.18}$$

The particle velocities can be obtain by solving Eq. (4.17). Once the velocity is known it is trivial to write down the equations of motion, which in the sheared frame are

$$\begin{cases} \dot{\mathbf{x}} = u_{ix} - \gamma u_{iy}, \\ \dot{\mathbf{y}} = u_{iy}. \end{cases} \tag{4.19}$$

When simulating Eq. (4.19) one never needs to calculate the inverse of the matrix $\mathbb{A}$ explicitly, which would be very time consuming. Instead one applies an iterative solver to (4.17), which is faster, but still takes significantly more computations than the other models that can be solved explicitly without any matrices. In paper V we show that in some cases it is possible to approximate the solutions of the $\mathrm{CD}_0$ model using the much faster non-overdamped model CD described in 4.6.1.

### 4.5.2 The $\mathrm{RD}_0$ model

The second version of the model introduced by Durian is a mean field version of the $\mathrm{CD}_0$ model, where instead of actually summing over the neighboring particles in Eq. (4.11) we replace the sum with an estimated average velocity of the neighboring particles $\langle \mathbf{v} \rangle$,

$$\mathbf{f}_i^{\mathrm{dis}} = -k_d z \left( \mathbf{v}_i - \langle \mathbf{v} \rangle \right). \tag{4.20}$$

Here $z$ is the average number of contacts per particle. This number is hard to know in advance so in the simulation we use $z = 1$. From the results it is then possible to calculate the true $z$ which tells us the effective $k_d$ of the simulation. There is an alternative interpretation of this model which justifies the use of $z = 1$: one could see the dissipation as not acting between contacting particles but instead be proportional to the velocity difference between the particle and the flow velocity of the surrounding medium $\mathbf{v}_{\mathrm{RD}}$ which serves as a velocity reservoir. In this case we imagine that the particles are immersed in a viscous liquid, and the dissipation would effectively be the normal Stoke's drag. The dissipative force then looks like

$$\mathbf{f}_i^{\mathrm{dis}} = -k_d \left( \mathbf{v}_i - \mathbf{v}_{\mathrm{RD}} \right). \tag{4.21}$$

The velocity of the background liquid $\mathbf{v}_{\mathrm{RD}}$ (or similarly $\langle \mathbf{v} \rangle$) is assumed to be a perfect Couette shear flow, given by $\mathbf{v}_{\mathrm{RD}} = \dot{\gamma} y_i \hat{\mathbf{x}}$ From the numerical point of view, the actual simulation is the same for both of these methods, the only difference is the post-processing, if one chooses to rescale the results to adjust for the $z$ factor or not. In the articles we have used this second interpretation of the dissipative force.

Written in shear frame coordinates the equations of motion become:

$$\begin{cases} \dot{x}_i = u_{ix} - \gamma u_{iy} = \frac{1}{k_d z} \left( f_{ix}^{el} - \gamma f_{iy}^{el} \right), \\ \dot{y}_i = u_{iy} = \frac{1}{k_d z} f_{iy}^{el}. \end{cases} \tag{4.22}$$

Here the $z$ factors have been included for completeness, but in practice all our simulation have been done with $z = 1$. The act of keeping $z$ constant means that the strength of the dissipation no longer varies with $\phi$.

### 4.5.3 Differences between the $\mathrm{CD}_0$- and $\mathrm{RD}_0$ models

In earlier work, Olsson and Teitel [8] showed that for the $\mathrm{RD}_0$ model it is possible to extract a shear rate dependent length scale from the spatial velocity correlation:

$$g_y(x) = \frac{\langle v_y(x_i, y_i) v_y(x_i + x, y_i) \rangle}{\langle v_y(x_i)^2 \rangle} \tag{4.23}$$

where $v_y(x, y)$ is the $y$ component of the velocity field at $(x, y)$, and the function $g(x)$ is the autocorrelation of $v_y$ along the $x$-direction and averaged over all particles. This length scale was shown to diverge as one approaches point J, indicating that point J is a critical point. However, Tighe et al. [28] noted that the velocity correlations in the $\mathrm{CD}_0$ models are very different, and that they lack a diverging length scale as point J is approached. Figure 4.8 shows the velocity correlation for the two models and how it depends on the shear rate. This raises the question: Does the type of dissipative mechanism in the

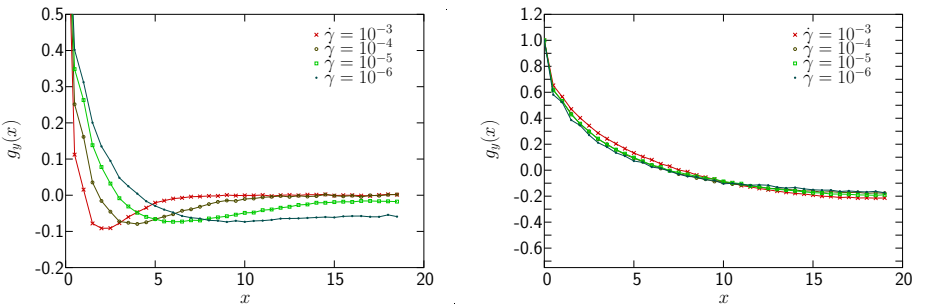


(a) $RD_0$ (b) $CD_0$

Figure 4.8: The normalized velocity correlation function $g_y(x)$ for different values of $\dot{\gamma}$ for a system with $N = 1024$ particles at $\phi = 0.8$. a) Data for the $RD_0$ model, here we observe a minimum in the curves which can be used to define a correlation length. This length diverges as the shear rate $\dot{\gamma} \to 0$. b) Data for the $CD_0$ model, here there is no minimum, and the correlation length seem to be almost independent of the shear rate.

system affect the critical behavior close to point J? In order to answer this question we decided to investigate several models with different dissipative forces. We also included mass to be able to determine what properties in the models change as we go to the overdamped limit.

In paper V we provide evidence that the critical behavior, close to the jamming transition, for both the $RD_0$ and $CD_0$ models are very similar. We have however not yet found the complete answer on what changes that can be made to the dissipative force without altering the observed critical behavior.

## 4.6 Adding Mass to the Simulations

We are now going to reintroduce mass to the Durian bubble model. As described above one reason for investigating these models was to see if the difference, as seen in figure 4.8, observed between the velocity correlation functions for the $RD_0$ and $CD_0$ model still remain when we have massive particles, and also to investigate in which parame-

ter ranges the models with mass agree with the overdamped models. However, it turns out that the behavior of these models is highly dependent on the choice of parameter values and we have observed a lot of interesting effects away from the overdamped limit that we originally were interested in when starting the work on paper IV and V.

In these models each particle now has a finite mass $m_i$. The equation of motion is then simply Newton's second law,

$$m_i \ddot{\mathbf{r}}_i = \mathbf{f}_i^{\text{el}} + \mathbf{f}_i^{\text{dis}}. \tag{4.24}$$

Written in the sheared coordinates and modified velocities one gets

$$\begin{cases} \dot{x}_i = u_{ix} - \gamma u_{iy}, \\ \dot{y}_i = u_{iy}, \\ \dot{u}_{ix} = \frac{1}{m_i}\left(f_{ix}^{\text{el}} + f_{ix}^{\text{dis}}\right) - \dot{\gamma} u_{iy}, \\ \dot{u}_{iy} = \frac{1}{m_i}\left(f_{iy}^{\text{el}} + f_{iy}^{\text{dis}}\right), \end{cases} \tag{4.25}$$

which is known as the SLLOD equations of motions [29] [18].

### 4.6.1 The CD model

for the CD model we use the same dissipation as in the $\text{CD}_0$ model, i.e. the dissipative force $\mathbf{f}_i^{\text{dis}}$ is proportional to the relative velocity between contacting particles:

$$\mathbf{f}_i^{\text{CD}} = -k_d \sum_{r_{ij}<d_{ij}} \left(\mathbf{v}_i - \mathbf{v}_j\right). \tag{4.26}$$

We can rewrite the force in terms of the modified velocity which gives

$$\mathbf{f}_i^{\text{CD}} = -k_d \sum_{r_{ij}<d_{ij}} \left(\mathbf{u}_i - \mathbf{u}_j + \dot{\gamma}\left[y_i - y_j\right]_{L_y} \hat{\mathbf{x}}\right). \tag{4.27}$$

The notation $[y_i - y_j]_{L_y}$ stands for the shortest distance between $i$ and $j$ in the $y$ direction, considering the periodic boundary conditions.

Inserting the force into the equation of motions gives

$$\begin{cases} \dot{x}_i = u_{ix} - \gamma u_{iy}, \\ \dot{y}_i = u_{iy}, \\ \dot{u}_{ix} = \frac{f_{ix}^{el}}{m_i} - \frac{k_d}{m_i} \sum_j' \left( u_{ix} - u_{jx} + \dot{\gamma} \left[ y_i - y_j \right]_{L_y} \right) - \dot{\gamma} u_{iy}, \\ \dot{u}_{iy} = \frac{f_{iy}^{el}}{m_i} - \frac{k_d}{m_i} \sum_j' \left( u_{iy} - u_{jy} \right), \end{cases} \tag{4.28}$$

where the sums run of all particles $j$ in contact with $i$.

### 4.6.2 The $\mathrm{CD}_n$ model

The dissipation in the CD model used the relative velocity. We now limit the dissipation to only act on the normal component of the relative velocity. This type of dissipation is often used to model massive granular particles [30,31]. An interesting difference between this model and the overdamped models like $\mathrm{RD}_0$ and $\mathrm{CD}_0$ is that the rheology below jamming is now Bagnoldian, $\sigma \sim \dot{\gamma}^2$. A reason why we are interested in this model, is that it will help us determine what properties of the particle interaction that are important in order to get Newtonian or Bagnoldian rheology.

We use the following expression for the dissipative force:

$$\mathbf{f}_i^{\mathrm{CD}_n} = -k_d \sum_{r_{ij} < d_{ij}} \left[ (\mathbf{v}_i - \mathbf{v}_j) \cdot \hat{\mathbf{r}}_{ij} \right] \hat{\mathbf{r}}_{ij}. \tag{4.29}$$

The equations of motion can be obtained by substituting $\mathbf{f}_i^{\mathrm{diss}}$ with $\mathbf{f}_i^{\mathrm{CD}_n}$ in Eq. (4.25).

### 4.6.3 The $\mathrm{CD}_t$ model

We can also define a dissipation to only act on the tangential component of the relative velocity:

$$\mathbf{f}_i^{\mathrm{CD}_t} = \mathbf{f}_i^{\mathrm{CD}} - \mathbf{f}_i^{\mathrm{CD}_n}. \tag{4.30}$$

This model has, to the best of our knowledge, not been studied before. It might be difficult to find a physical system that behaves according to this dissipation, however from a theoretical point of view this model has been very useful in understanding the difference between the CD and $\mathrm{CD}_n$ model.

### 4.6.4 The RD model

We can also add mass to the $\mathrm{RD}_0$ model. We then use the same dissipation as for $\mathrm{RD}_0$:

$$\mathbf{f}_i^{\mathrm{dis}} = -k_d \left( \mathbf{v}_i - \mathbf{v}_{\mathrm{RD}} \right), \tag{4.31}$$

which we can insert in equation (4.25) to get the equations of motion,

$$\begin{cases} \dot{x}_i = u_{ix} - \gamma u_{iy}, \\ \dot{y}_i = u_{iy}, \\ \dot{u}_{ix} = \frac{f_{ix}^{el}}{m_i} - \frac{k_d}{m_i} u_{ix} - \dot{\gamma} u_{iy}, \\ \dot{u}_{iy} = \frac{f_{iy}^{el}}{m_i} - \frac{k_d}{m_i} u_{iy}. \end{cases} \tag{4.32}$$

The same discussion as for the $\mathrm{RD}_0$ model regarding whether to replace $k_d$ with $k_d z$ in the dissipative force applies here as well and depends on which interpretation we use for the dissipative force.

## 4.7 Energy Minimization and the Quasistatic-Limit

The limit when $\dot{\gamma} \to 0$ is known as the quasistatic-limit. This limit is interesting since we would like to get data as close as possible to the critical point J. Approaching this limit using a finite $\dot{\gamma}$ is difficult since the time it takes the system to shear a certain amount $\gamma$ is directly proportional to $\dot{\gamma}$. With the currently available computer resources it is possible to do simulations down to $\dot{\gamma} \sim 10^{-9}$. More and faster computers will of course lower this limit, but there are more efficient methods of obtaining the limiting value. What we would

like to do is to give the system time to relax completely between each shear increment. This is however a very slow process since the relaxation times close to jamming can be very long [32]. The approach we use instead is to do quasistatic shearing by numerically minimizing the energy of the particle configuration in between each small shear increment $\Delta\gamma$. The algorithm for doing quasistatic shearing is simply

1. Repeat until done:
2. Shear system $\gamma \to \gamma + \Delta\gamma$
3. Minimize energy of system

Here it is important to note that since we use the numerical minimization we can not say how long physical time it would have taken for the system to reach the minimized state using the normal dynamics, and consequently we do not know how long time it is between successive shear steps. This is also why we use the notation $\Delta\gamma$ instead of $\dot{\gamma}$, which would imply that there is a known time interval between successive steps. If $\Delta\gamma$ is small enough, the resulting dynamics is independent of the exact value of $\Delta\gamma$, which means that we have reached the quasistatic limit. For the minimization we used the Polak-Ribiere method [33], which is a non-linear conjugate gradient method, see the appendix of paper I for more details on the minimization. One thing to remember when using this type of minimizing routines is that the particles will not follow the exact same paths as if the system was allowed to relax using the normal dynamics, which means that when looking at a specific configuration the final energy after minimization/relaxation will differ. However, on average, when considering the average minimized energy over a large collection of particle configurations, the two methods agree.

Another issue to consider when modeling particles configurations with very small overlaps is the numerical accuracy, especially when using iterative methods like this. For example, in order to get the whole system of particles to minimize uniformly, all particles should have the same degrees of freedom. This is not the case if the particle coordinates are represented using ordinary floating point variables. Due to

the nature of floating point variables, the position of particles close to the origin can be specified more accurately than the position of particles far from the origin. This can be seen as a force gradient across a minimized system. The effect is however only seen when minimizing to very low energies, the onset of this effect depends on the system size and it can usually be ignored for smaller systems. The system sizes used in the included papers were all small enough that this effect did not affect the jammed states in any significant way. The effect can however be seen if studying the low energy unjammed states, but that is no problem since they were never used in the analysis. It is possible to eliminate this effect by making sure that all particle coordinates have the same resolution. One way of doing this is to split the coordinate $r$ of a particle into two parts $r = r_b + r_o$, where $r_b$ is the base giving the rough position of the particle and $r_o$ is an offset from the base position. Since minimization only involves small displacements, the $r_b$ value can be set at the beginning of each minimization, and any changes to the particle position can then be performed on $r_o$. Using this method all particles behave the same regardless of their position within the system.

# Chapter 5

# Criticality and Scaling

Critical scaling is a phenomenon that can be observed close to critical points or critical lines in parameter space. These critical points (or lines) are associated with continuous phase transitions and constitute the boundary between two phases in such a transition. Close to the phase transition many properties of the system exhibit power-law dependencies. Using Renormalization group theory we can explain this behavior and explain the behavior in terms of scaling relations that describe how an observable in the system transforms if the length scale of the system changes. The main idea is that there exists a correlation length $\xi$ in the system, and as we approach the critical point, $\xi$ diverges. This means that at the critical point the whole system is correlated and fluctuations occur at all length scales. The system is then said to be scale-free.

The renormalization group was initially devised in particle physics, but nowadays its applications extend to solid-state physics, fluid mechanics, cosmology and even nanotechnology. In the study of equilibrium phase transitions scaling theory is well established and has seen extensive use especially in different types of spin systems. Applying multivariable critical scaling to the athermal jamming transition, a non-equilibrium transition, which presently lacks a solid theoretical foundation, is a fairly new approach. The first use of these methods in the context of jamming were by Olsson and Teitel in 2007 [8].

## 5.1 Scaling around point J

Sufficiently close to point J we can formulate a scaling assumption that predicts how an observable (e.g. shear stress, pressure, energy, and jamming fraction) will behave if we rescale the system with a scale factor $b$. For athermal systems, $T = 0$, sheared at a constant shear strain rate $\dot{\gamma}$, in the vicinity of the critical point J we expect an observable $\mathcal{O}$ to scale as

$$\mathcal{O}(\phi, \dot{\gamma}, L) = b^{-y_{\mathcal{O}}/\nu} f\left((\phi - \phi_J)\, b^{1/\nu}, \dot{\gamma} b^z, L^{-1} b\right), \tag{5.1}$$

where $L$ is the system length, $f$ is an unknown scaling function and $b$ is an arbitrary scale factor. We will explain the use of $f$ and $b$ shortly. Here $y_{\mathcal{O}}$, $\nu$ and $z$ are the critical exponents describing the behavior close to point J. The critical exponent $y_{\mathcal{O}}$ is associated with the specific observable and may be different for different observables, the exponent $\nu$ is the correlation length critical exponent, and $z$ is the dynamical critical exponent. The exponents $\nu$ and $z$ are assumed to be the same for all observables. The scaling function $f$ depends on three parameters $\phi$, $\dot{\gamma}$ and $L$, this is a very general expression and in order to more easily analyze the system behavior one usually looks at limiting cases where two of the three parameters have known values. We are free to select the scale factor $b$ however we like, and we will use this freedom to cancel one of the parameters in $f$.

## 5.2 Scaling in the limit $L \to \infty$

If we take $b = \dot{\gamma}^{-1/z}$ the second parameter in the scaling function $f$, equation (5.1), becomes a constant. If we then look at the limit $L \to \infty$, which takes the third parameter to zero, we get the following scaling relation

$$\mathcal{O}(\phi, \dot{\gamma}) = \dot{\gamma}^{y_{\mathcal{O}}/z\nu} f\left((\phi - \phi_J)/\dot{\gamma}^{1/z\nu}, 1, 0\right). \tag{5.2}$$

This relation tells us that if we plot $\mathcal{O}/\dot{\gamma}^{y_{\mathcal{O}}/z\nu}$ vs. $(\phi - \phi_J)/\dot{\gamma}^{1/z\nu}$ all points in the two-dimensional $(\phi, \dot{\gamma})$ plane will collapse to a sin-

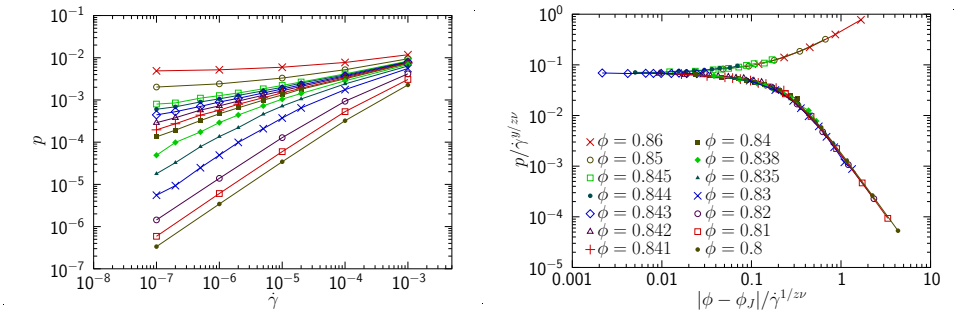


(a) Raw data

(b) Collapsed data

Figure 5.1: Example of scaling collapse of data in the $(\phi, \dot{\gamma})$-plane. Since $\phi - \phi_J$ changes sign at $\phi_J$ we use the magnitude of $\phi - \phi_J$ in order to see both branches in the log-log plot. Data for $\mathrm{RD}_0$-model with $N = 1024$ particles, using $\phi_J = 0.8433$, $y = 1.1$, and $z\nu = 3.5$.

gle curve, as illustrated in figure 5.1. We can continue to reduce the number of variables further by looking at the behavior exactly at the critical jamming density, $\phi = \phi_J$. The scaling function is now a constant, $f(0, 1, 0)$, and we expect

$$\mathcal{O} \sim \dot{\gamma}^{q_\mathcal{O}} \text{ at } \phi = \phi_J, \tag{5.3}$$

where $q_\mathcal{O} = y_\mathcal{O}/z\nu$. This corresponds to a non-linear rheology. Similarly, we can look at the $\phi$-dependence above and below $\phi_J$, in the limit $\dot{\gamma} \to 0$. Below jamming, $\phi < \phi_J$, we expect the rheology to be linear if $\dot{\gamma}$ is small enough. In order to get linear rheology in the limit $\dot{\gamma} \to 0$, the scaling function $f(x, 1, 0)$ should be proportional to $x^{y_\mathcal{O} - z\nu}$ as $x \to -\infty$, which gives

$$\frac{\mathcal{O}}{\dot{\gamma}} \sim |\phi - \phi_J|^{-\beta_\mathcal{O}} \text{ for } \phi < \phi_J, \tag{5.4}$$

where the exponent is $\beta_\mathcal{O} = z\nu - y_\mathcal{O}$.

For $\phi > \phi_J$, above jamming, we expect a finite yield stress which suggests that all observables should be independent of $\dot{\gamma}$ in the limit

$\dot{\gamma} \to 0$. This implies that the scaling function $f(x, 1, 0)$ must be proportional to $x^{y_\mathcal{O}}$, which gives

$$\mathcal{O} \sim (\phi - \phi_J)^{y_\mathcal{O}} \text{ for } \phi > \phi_J. \tag{5.5}$$

## 5.3 Finite Size Scaling

In the above, we assumed that we had a really large system so that any finite size effects can be neglected. However, obtaining good data for large systems is computationally expensive. An alternative way of approaching the problem is to study how system properties change with system size. It is then possible to use data for smaller system sizes which are affected by finite size effects, and through the use of scaling relations determine the critical exponents.

We start from the same scaling assumption as before, Eq. (5.1), however this time we select $b = L$. In the limit $\dot{\gamma} \to 0$ this becomes

$$\mathcal{O}(\phi, \dot{\gamma}, L) = L^{y_\mathcal{O}/\nu} f\left(\frac{(\phi - \phi_J)}{L^{1/\nu}}, 0, 1\right). \tag{5.6}$$

An advantage of using finite size scaling is that we can determine the $\nu$ exponent separately, which is in contrast to the scaling analysis described above where it only appeared in the combination $z\nu$. By doing both of these scaling analyses together we can determine the values of both $z$ and $\nu$.

## 5.4 Correction to Scaling

For many phase transitions it could seem to be fairly straight-forward to determine the exponents and the location of the critical point by fitting data to the type of scaling expressions discussed in the previous sections. However, for the jamming transition the situation is a bit more complicated, as it turns out that the scaling assumption (5.1) we

started with is somewhat too simple. The scaling function $f$ in equation (5.1) does in fact take more arguments than what we explicitly show here. The complete expression would look like

$$\mathcal{O}\left(\mu_1, ..., \mu_n\right) = b^{-y_\mathcal{O}/\nu} f\left(\mu_1 b^{y_1}, ..., \mu_n b^{y_n}\right), \tag{5.7}$$

where the state of the system is given by the set of parameters $\mu_1, ..., \mu_n$. The reason to exclude most of these parameters is that they constitute irrelevant variables. An irrelevant variable describes a property of the system that decreases in importance as the system is rescaled with a factor $b > 1$, reducing the number of degrees of freedom in the system. Relevant variables on the other hand are properties that remains important after rescaling, in our case $\phi$, $\dot{\gamma}$, and $L$. Mathematically, a parameter $\mu_i$ is relevant if the corresponding exponent is $y_i > 0$, and irrelevant if $y_i < 0$. Exactly at the critical point only relevant variables remain after rescaling, however, if we are not exactly at the critical point there might still be contributions from some of the irrelevant variables. The idea is that if we are close enough to the critical point the scaling expression in equation (5.1) should hold as the contribution from the irrelevant variables can be neglected. However what constitutes "close enough" is usually not known in advance. It turns out that for the jamming transition we often need to include a correction term, which includes the effect of the largest remaining irrelevant variable, in order to get good agreement between the data and theory. When we add this term the scaling assumption changes to

$$\begin{aligned}\mathcal{O}\left(\phi, \dot{\gamma}, L\right) = b^{-y_\mathcal{O}/\nu}\big[ & f_0\left(\left(\phi - \phi_J\right) b^{1/\nu}, \dot{\gamma} b^z, L^{-1} b\right) \\ & + b^{-\omega} f_1\left(\left(\phi - \phi_J\right) b^{1/\nu}, \dot{\gamma} b^z, L^{-1} b\right)\big],\end{aligned} \tag{5.8}$$

where we now have two scaling functions, $f_0$ and $f_1$, and a new critical exponent $\omega$ associated with the second term. Note that we do not need to know which parameter "$\mu$" that we are correcting for in order to use this method. Including this second term in the scaling expression is known as using corrections to scaling [34] [35]. In Ref. [36] Olsson

and Teitel show that such corrections need to be included, they also show that the correction term is larger for the shear stress $\sigma$ than for the pressure $p$. That is why we choose to mainly look at pressure rather than shear stresses in the subsequent works.

# Chapter 6

# Summary of Papers

Here follows a short description of the publications included in this thesis. Since all of the papers have multiple authors a short description of my contribution to each paper is also included. A significant part of my work has concerned the development and testing of numerical simulation software, running the software, data management, and doing statistical post-processing of the output. However all articles have been written in close collaboration, which means that I have had the opportunity to provide input at all stages during the production of the manuscripts.

## 6.1 Paper I

**Glassiness, Rigidity, and Jamming of Frictionless Soft Core Disks**

In this paper we investigate how the jamming probability of a configuration of particles depends on the way it was generated. A configuration is considered jammed if the energy per particle after quenching is larger than a small cut-off value $e_{\text{cut}} = 10^{-16}$. We generate a large number of configurations using several different protocols, the configurations are then quenched to determine what fraction of them that jam. We find that cooling followed by compression leads to a wide distribution of jamming packing fractions $\phi_J$, that depends on both the cooling rate and the initial properties of the configuration. We show that shearing gives a narrower distribution of $\phi_J$, and attribute this difference to the mixing that occurs during shear which prevents phase separation of large and small particles, i.e. the formation of

larger monodisperse regions in an otherwise bidisperse system. This makes the sheared ensemble independent of the initial configuration. We conclude that shear-driven jamming is a unique and well-defined critical point.
**contribution:** *Extensive developments of the numerical methods for both minimizations with the conjugate gradient method and quasistatic shearing simulations as detailed in Appendix A. Performed all the numerical simulations except the Hard-Core simulations in section D.*

## 6.2 Paper II

**Finite-Size Scaling at the Jamming Transition: Corrections to Scaling and the Correlation-Length Critical Exponent**
In this paper we perform a finite size scaling analysis. We compare the result from two ensembles, RAND where we quench starting from random initial positions, and QS obtained from quasistatic shearing. We determine the spatial correlation length exponent $\nu$ and show that corrections to scaling must be included when analyzing the data in order to get correct results. Including corrections to scaling gives a significantly higher value of $\nu$ than have been reported in earlier work that did not consider corrections to scaling [11].
**contribution:** *All the numerical simulations and I was also involved in several attempts at analyzing the data with finite size scaling.*

## 6.3 Paper III

**Pressure Distribution and Critical Exponent in Statically Jammed and Shear-Driven Frictionless Disks**
In this paper we study the distribution of pressures of configurations from the RAND- and QS-ensembles. For the RAND ensemble we use both harmonic and Hertzian particle interactions. When approaching the jamming transition from above we expect the pressure to scale

as $p \sim (\phi - \phi_J)^y$. We show a simple way of determining if the pressure critical exponent is $y > 1$ or $y \leq 1$ based on a divergence in the pressure distribution. We confirm that $y > 1$ for the QS-ensemble as expected from previous work based on simulations at constant shear rate [36].
**contribution:** *Numerical simulations, both quasistatic shearing and minimizations for the harmonic RAND ensemble.*

## 6.4 Paper IV

### Dissipation and Rheology of Sheared Soft-Core Frictionless Discs Below Jamming

The background of this paper was the intriguing observation that granular particles are usually found to obey Bagnoldian scaling whereas foams and emulsions are found to obey Newtonian scaling. We therefore set out to compare the rheology of the RD, CD, $\text{CD}_n$ and $\text{CD}_t$ models. We investigate which of these models have a well-defined overdamped limit, and which criteria that must be fulfilled in order to get an overdamped dynamics. We note that several of these models can exhibit both Newtonian rheology and Bagnoldian rheology depending on the relation between the parameters $k_e$, $k_d$ and $m$, and that there in some cases seem to be sharp transitions between the two types of rheology. We find that the Newtonian rheology is associated with the formation of large particle clusters, while in the Bagnoldian regime particles separate after contact and no large clusters are observed.
**contribution:** *All the numerical simulations and I was also deeply involved in the development of the theory.*

## 6.5 Paper V

### Universality of Jamming Criticality in Overdamped Shear-Driven Frictionless Disks

Here we compare the $RD_0$ and the $CD_0$ models. We investigate the claims by Tighe et al. [28] regarding the different scaling behavior of the $RD_0$ and the $CD_0$ models. We present an argument for why the velocity correlations are so different, and show that both models seem to scale the same way close to the jamming transition in the overdamped limit. We show that it is possible to use data from the much faster CD model with finite $m$, simulated in the overdamped limit, in place of "real" overdamped data from the slower $CD_0$ model where $m = 0$.

**contribution:** *All simulations for the CD model and I was also involved in the analyses, at an early stage especially on the crucial question on the velocity correlations which were then calculated with zero mass, and later also on the divergence of the pressure as point J is approached.*

# Acknowledgments

This thesis would not have been possible without the guidance from my advisors Peter Olsson and Steve Teitel, whose help, support, discussions and innumerable emails kept this work on track.

I would also like to thank my friends and family for supporting me during this time. Special thanks to Sofie Öhberg, Per Vågberg, Mattias and Maja Vågberg. Also many thanks to all the nice people at the Physics department of which there are too many to provide a complete list. I especially thank Johan Zakrisson, Andreas Sandström, Avazeh Hashemloo, Nargis Mortezaei, Jenny Enevold and Isak Silander for fun times and interesting conversations.

I would also like to thank Swedish National Infrastructure for Computing (SNIC) at PDC and HPC2N for providing the computational resources that made this work possible.

And of course, last but definitely not least, I would like to thank my parents.

# References


[1] M. Pakpour, M. Habibi, P. Mller, and D. Bonn, How to construct the perfect sandcastle, Sci. Rep. **2**, (2012).

[2] P. G. de Gennes, Granular matter: a tentative view, Rev. Mod. Phys. **71**, S374 (1999).

[3] I. Zuriguel, A. Garcimartín, D. Maza, L. A. Pugnaloni, and J. M. Pastor, Jamming during the discharge of granular matter from a silo, Phys. Rev. E **71**, 051303 (2005).

[4] E. Steltz, A. Mozeika, J. Rembisz, N. Corson, and H. M. Jaeger, Jamming as an enabling technology for soft robotics, Proc. SPIE **7642**, 764225 (2010).

[5] A. J. Liu and S. R. Nagel, Jamming is Not Just Cool Any More, Nature (London) **396**, 21 (1998).

[6] A. Ikeda, L. Berthier, and P. Sollich, Unified study of glass and jamming rheology in soft particle systems, Phys. Rev. Lett. **109**, 018301 (2012).

[7] P. Olsson and S. Teitel, Athermal jamming versus thermalized glassiness in sheared frictionless particles, Phys. Rev. E **88**, 010301 (2013).

[8] P. Olsson and S. Teitel, Critical scaling of shear viscosity at the jamming transition, Phys. Rev. Lett. **99**, 178001 (2007).

[9] C. Heussinger and J.-L. Barrat, Jamming Transition as Probed by Quasistatic Shear Flow, Phys. Rev. Lett. **102**, 218303 (2009).

[10] J. Paredes, M. A. J. Michels, and D. Bonn, Rheology across the Zero-Temperature Jamming Transition, Phys. Rev. Lett. **111**, 015701 (2013).

[11] C. S. O'Hern, L. E. Silbert, A. J. Liu, and S. R. Nagel, Jamming at zero temperature and zero applied stress: The epitome of disorder, Phys. Rev. E **68**, 011306 (2003).

[12] D. Bideau and J. P. Troadec, Compacity and mean coordination number of dense packings of hard discs, Journal of Physics C: Solid State Physics **17**, L731 (1984).

[13] A. Donev, I. Cisse, D. Sachs, E. A. Variano, F. H. Stillinger, R. Connelly, S. Torquato, and P. M. Chaikin, Improving the Density of Jammed Disordered Packings Using Ellipsoids, Science **303**, 990 (2004).

[14] W. Man, A. Donev, F. H. Stillinger, M. T. Sullivan, W. B. Russel, D. Heeger, S. Inati, S. Torquato, and P. M. Chaikin, Experiments on Random Packings of Ellipsoids, Phys. Rev. Lett. **94**, 198001 (2005).

[15] Z. Zeravcic, N. Xu, A. J. Liu, S. R. Nagel, and W. van Saarloos, Excitations of ellipsoid packings near jamming, EPL (Europhysics Letters) **87**, 26001 (2009).

[16] E. Bingham, An investigation of the laws of plastic flow, Bulletin of the Bureau of Standards **13**, 309 (1916).

[17] R. A. Bagnold, Experiments on a Gravity-Free Dispersion of Large Solid Spheres in a Newtonian Fluid under Shear, Proceedings of The Royal Society A: Mathematical, Physical and Engineering Sciences **225**, 49 (1954).

[18] D. Evans and G. Morriss, *Statistical Mechanics of Nonequilibrium Liquids*, *Theoretical chemistry* (Cambridge University Press, Cambridge, 2008).

[19] J. Williams, The segregation of particulate materials. A review, Powder Technology **15**, 245 (1976).

[20] D. N. Perera and P. Harrowell, Stability and structure of a supercooled liquid mixture in two dimensions, Phys. Rev. E **59**, 5721 (1999).

[21] R. J. Speedy, Glass transition in hard disc mixtures, The Journal of Chemical Physics **110**, 4559 (1999).

[22] A. Panaitescu, K. A. Reddy, and A. Kudrolli, Nucleation and Crystal Growth in Sheared Granular Sphere Packings, Phys. Rev. Lett. **108**, 108001 (2012).

[23] L. D. Landau, E. M. Lifshits, A. M. Kosevich, and L. P. Pitaevskii, *Theory of elasticity* (Butterworth-Heinemann, Oxford [England]; New York, 1986).

[24] C. S. O'Hern, S. A. Langer, A. J. Liu, and S. R. Nagel, Random packings of frictionless particles, Phys. Rev. Lett. **88**, 075507 (2002).

[25] P. Allen and D. Tildesley, *Computer Simulation of Liquids*, *Oxford Science Publ* (Clarendon Press, Oxford, 1989).

[26] E. Lerner, G. Düring, and M. Wyart, Simulations of driven overdamped frictionless hard spheres, Computer Physics Communications **184**, 628 (2013).

[27] D. J. Durian, Foam Mechanics at the Bubble Scale, Phys. Rev. Lett. **75**, 4780 (1995).

[28] B. P. Tighe, E. Woldhuis, J. J. C. Remmers, W. van Saarloos, and M. van Hecke, Model for the Scaling of Stresses and Fluctuations in Flows near Jamming, Phys. Rev. Lett. **105**, 088303 (2010).

[29] D. J. Evans and O. Morriss, Non-Newtonian molecular dynamics, Computer Physics Reports **1**, 297 (1984).

[30] D. E. W. J. Schäfer, S. Dippel, Force Schemes in Simulations of Granular Materials, J. Phys. I France **6**, 5 (1996).

[31] M. Otsuki and H. Hayakawa, Critical behaviors of sheared frictionless granular materials near the jamming transition, Phys. Rev. E **80**, 011308 (2009).

[32] T. Hatano, Growing length and time scales in a suspension of athermal particles, Phys. Rev. E **79**, 050301 (2009).

[33] W. Press, *Numerical Recipes 3rd Edition: The Art of Scientific Computing* (Cambridge University Press, Cambridge, 2007).

[34] F. J. Wegner, Corrections to Scaling Laws, Phys. Rev. B **5**, 4529 (1972).

[35] M. E. Fisher, The renormalization group in the theory of critical behavior, Rev. Mod. Phys. **46**, 597 (1974).

[36] P. Olsson and S. Teitel, Critical Scaling of Shearing Rheology at the Jamming Transition of Soft Core Frictionless Disks, Phys. Rev. E **83**, 030302(R) (2011).